Long range surface plasmon-coupled fluorescence emission for biosensor applications

Koji Toma, Jakub Dostalek,[*] **and Wolfgang Knoll**

AIT - Austrian Institute of Technology GmbH, Health and Environment Department, Muthgasse 11, 1190 Vienna, Austria

[*]jakub.dostalek@ait.ac.at

Abstract: A biosensor scheme that employs long range surface plasmons (LRSPs) for the efficient excitation and collection of fluorescence light from fluorophore-labeled biomolecules captured in a three-dimensional hydrogel matrix is discussed. This new approach to plasmon-enhanced fluorescence (PEF) is experimentally and theoretically investigated by using the Kretschmann configuration of attenuated total reflection (ATR) method. A layer structure supporting LRSPs that consists of a low refractive index fluoropolymer layer, a thin gold film and a large binding capacity N-isopropylacrylamide (NIPAAm)-based hydrogel matrix swollen in an aqueous sample is employed. By using this layer architecture, the extended field of LRSPs probes the binding of biomolecules in the binding matrix at up to micrometer distances from the gold surface. With respect to regular surface plasmon-enhanced fluorescence spectroscopy (SPFS) and surface plasmon-coupled emission (SPCE), a narrower angular distribution of the fluorescence light intensity, a larger peak intensity and the excitation and emission at lower angles were observed.

References and links

1. M. Seidel and R. Niessner, "Automated analytical microarrays: a critical review," Anal. Bioanal. Chem. **391**(5), 1521–1544 (2008).
2. M. E. Stewart, C. R. Anderton, L. B. Thompson, J. Maria, S. K. Gray, J. A. Rogers, and R. G. Nuzzo, "Nanostructured plasmonic sensors," Chem. Rev. **108**(2), 494–521 (2008).
3. J. R. Lakowicz, "Plasmonics in biology and plasmon-controlled fluorescence," Plasmonics **1**(1), 5–33 (2006).
4. J. Dostálek and W. Knoll, "Biosensors based on surface plasmon-enhanced fluorescence spectroscopy," Biointerphases **3**(3), FD12–FD22 (2008).
5. T. Liebermann and W. Knoll, "Surface-plasmon field-enhanced fluorescence spectroscopy," Colloids Surf. A Physicochem. Eng. Asp. **171**(1-3), 115–130 (2000).
6. J. R. Lakowicz, J. Malicka, I. Gryczynski, and Z. Gryczynski, "Directional surface plasmon-coupled emission: A new method for high sensitivity detection," Biochem. Biophys. Res. Commun. **307**(3), 435–439 (2003).
7. J. S. Yuk, M. Trnavsky, C. McDonagh, and B. D. MacCraith, "Surface plasmon-coupled emission (SPCE)-based immunoassay using a novel paraboloid array biochip," Biosens. Bioelectron. **25**(6), 1344–1349 (2010).
8. S. C. Kitson, W. L. Barnes, and J. R. Sambles, "Photoluminescence from dye molecules on silver gratings," Opt. Commun. **122**(4-6), 147–154 (1996).
9. D. Sarid, "Long-range surface-plasma waves on very thin metal-films," Phys. Rev. Lett. **47**(26), 1927–1930 (1981).
10. G. Winter, S. Wedge, and W. L. Barnes, "Can lasing at visible wavelength be achieved using the low-loss long range surface plasmon-polariton mode?" N. J. Phys. **8**(8), 125–138 (2006).
11. T. Okamoto, J. Simonen, and S. Kawata, "Plasmonic crystal for efficient energy transfer from fluorescent molecules to long-range surface plasmons," Opt. Express **17**(10), 8294–8301 (2009).
12. I. De Leon and P. Berini, "Amplification of long-range surface plasmons by a dipolar gain medium," Nat. Photonics **4**(6), 382–387 (2010).
13. A. Kasry and W. Knoll, "Long range surface plasmon fluorescence spectroscopy," Appl. Phys. Lett. **89**(10), 101106 (2006).
14. J. Dostálek, A. Kasry, and W. Knoll, "Long range surface plasmons for observation of biomolecular binding events at metallic surfaces," Plasmonics **2**(3), 97–106 (2007).

15. Y. Wang, A. Brunsen, U. Jonas, J. Dostálek, and W. Knoll, "Prostate specific antigen biosensor based on long range surface plasmon-enhanced fluorescence spectroscopy and dextran hydrogel binding matrix," Anal. Chem. **81**(23), 9625–9632 (2009).
16. Y. Wang, J. Dostálek, and W. Knoll, "Long range surface plasmon-enhanced fluorescence spectroscopy for the detection of aflatoxin M_1 in milk," Biosens. Bioelectron. **24**(7), 2264–2267 (2009).
17. C. J. Huang, J. Dostalek, and W. Knoll, "Optimization of layer structure supporting long range surface plasmons for surface plasmon-enhanced fluorescence spectroscopy biosensors," J. Vac. Sci. Technol. B **28**(1), 66–72 (2010).
18. C. J. Huang, J. Dostalek, and W. Knoll, "Long range surface plasmon and hydrogel optical waveguide field-enhanced fluorescence biosensor with 3D hydrogel binding matrix: on the role of diffusion mass transfer," Biosens. Bioelectron. **26**(4), 1425–1431 (2010).
19. A. Aulasevich, R. F. Roskamp, U. Jonas, B. Menges, J. Dostalek, and W. Knoll, "Optical waveguide spectroscopy for the investigation of protein-functionalized hydrogel films," Macromol. Rapid Commun. **30**(9-10), 872–877 (2009).
20. M. Daimon and A. Masumura, "Measurement of the refractive index of distilled water from the near-infrared region to the ultraviolet region," Appl. Opt. **46**(18), 3811–3820 (2007).
21. W. N. Hansen, "Electric fields produced by the propagation of plane coherent electromagnetic radiation in a stratified medium," J. Opt. Soc. Am. **58**(3), 380–388 (1968).
22. G. W. Ford and W. H. Weber, "Electromagnetic interactions of molecules with metal surfaces," Phys. Rep. **113**(4), 195–287 (1984).
23. L. Polerecký, J. Hamrle, and B. D. MacCraith, "Theory of the radiation of dipoles placed within a multilayer system," Appl. Opt. **39**(22), 3968–3977 (2000).
24. P. W. Beines, I. Klosterkamp, B. Menges, U. Jonas, and W. Knoll, "Responsive thin hydrogel layers from photo-cross-linkable poly(N-isopropylacrylamide) terpolymers," Langmuir **23**(4), 2231–2238 (2007).

1. Introduction

Over the last decade, increasing efforts were devoted to fluorescence-based detection of chemical and biological analytes [1] with advanced sensitivity by using plasmon-enhanced fluorescence (PEF) [2–4]. Surface plasmons (SPs) are optical waves that originate from coupled collective oscillations of electron plasma and associated electromagnetic field at a metallic surface. Up to now, two main approaches that rely on SPs propagating along continuous metallic films were pursued for PEF. In surface plasmon-enhanced fluorescence spectroscopy (SPFS) [5], the binding of fluorophore-labeled molecules to biomolecular recognition elements attached on a metallic sensor surface is probed by the enhanced field intensity of SPs. This method takes advantage of increased excitation rate of fluorophores that is directly translated to an enhanced fluorescence signal. In surface plasmon-coupled fluorescence emission (SPCE) [6], fluorescence light emitted by fluorophores via SPs is detected. The out-coupling of fluorescence light that is trapped in SPs to far field radiation by using hemispherical [6] and parabolic [7] dielectric elements and metallic diffraction gratings [8] was reported to provide efficient means for collecting of SPCE signal. Owing to the evanescent profile of the SP electromagnetic field, only the fluorescence signal originating from fluorophores in a close proximity to the metallic surface (distance up to ~100 nm) is detected by SPFS and SPCE methods leading to a greatly suppressed background.

In this paper, we investigate the excitation and emission of fluorophore-labeled biomolecules on a sensor surface that is supporting long range surface plasmons (LRSPs). These surface plasmon modes propagate along a thin metallic film that is embedded in dielectrics with similar refractive indices. They exhibit lower losses and an evanescent field that probe deeper away from a metallic surface compared to regular SPs [9]. The coupling of fluorophores with LRSPs was subject to theoretical investigation [10,11] and recently it found applications in areas including plasmonic lasers [12] and SPFS biosensors [13]. In the biosensor applications, LRSPs are particularly attractive for probing biointerfaces with an extended three-dimensional hydrogel matrix that offer a large binding capacity [14] and allowed for the detection of molecular analytes at low femtomolar concentrations in real samples [15,16]. In order to push forward the sensitivity of this biosensor scheme, we experimentally and theoretically study the excitation and emission of fluorescence light from dye molecules dispersed in a hydrogel binding matrix via LRSPs. The implementation of this method for more efficient and simpler detection of the fluorescence light is discussed.

2. Materials and methods

2.1 Materials

Cytop fluoropolymer (CTL-809M, 9 wt % in the solvent of CT-solv 180) was purchased from Asahi Glass (Japan). Phosphate buffered saline (PBS) with pH 7.4 was obtained from Calbiochem (Germany). PBS-Tween (PBS-T) buffer was prepared by adding 0.05% of Tween20 (Sigma-Aldrich, USA) to PBS buffer solution. Anti-mouse IgG (a-IgG) and mouse IgG (IgG) were from Molecular Probes (USA). a-IgG molecules were labeled with Alexa Fluor 647 with the dye-to-protein molar ratio of 4.5. This dye exhibits the quantum efficiency of $\eta = 0.33$ and the absorption and emission wavelengths at 650 nm and 668 nm, respectively. 10 mM acetate buffer (ACT) with pH 4 was prepared in house. 1-Ethyl-3-(3-dimethylaminopropyl) carbodiimide (EDC) was from Pierce (USA). Photocrosslinkable poly(*N*-isopropylacryamide) (NIPAAm)-based hydrogel with benzophenon and carboxylic groups, S-3-(benzoylphenoxy)propyl ethanthioate (benzophenone-thiol) and sodium *para*-tetrafluorophenol sulfonate (TFPS) were synthesized at Max Planck Institute for Polymer Research in Mainz, Germany. Ethanolamine (Sigma-Aldrich, USA) was dissolved in water at 1 M concentration with the pH of the solution adjusted to 8.5 with sodium hydroxide.

2.2 Preparation of sensor layer structures supporting LRSPs and regular SPs

The preparation of a layer structure supporting LRSP, grafting of a hydrogel binding matrix on its top and the immobilization of biomolecules were described in our previous works [17], [18]. Briefly, Cytop fluoropolymer film (thickness $d_{Cytop} = 655 \pm 15$ nm) was spin coated on a glass substrate followed by the deposition of gold layer (thickness $d_m = 18.9 \pm 1.7$ nm) by means of magnetron sputtering (UNIVEX 450C, Leybold Vacuum, Germany). For a comparison, a gold film (thickness $d_m = 47.2 \pm 0.8$ nm) was prepared on a glass substrate for the excitation of regular SPs. After the gold deposition, the surface of substrates supporting LRSP and regular SP was subsequently modified by benzophenon-thiol self-assembled monolayer (SAM), coated with NIPAAm-based hydrogel (thickness in a dry state of 60 nm) and exposed to UV light (an irradiation dose of 2 J cm^{-2} at a wavelength of $\lambda = 365$ nm) in order to photocrosslink the hydrogel film. As shown in our previous studies [19], the prepared NIPAAm-based hydrogel film swells in PBS-T buffer with the factor of around 10 leading to an increase in its thickness to $d_h \sim 600$ nm. Swollen hydrogel film was *in situ* functionalized with IgG molecules by the reacting of carboxylic groups in the gel with a mixture of EDC and TFPS followed by the covalent coupling of IgG molecules dissolved in ACT buffer via their amine moieties [19]. Afterwards, unreacted active ester groups of the hydrogel were passivated by the incubation in ethanolamine solution. Finally, fluorophore-labeled a-IgG molecules dissolved in PBS-T were flowed over the surface until the saturation of the affinity binding to immobilized IgG molecules was reached. The concentration of a-IgG that was captured in the gel was $c \sim 10^{-4}$ M which corresponds to the surface mass density $\Gamma = c/d_h \sim 10$ ng/mm^2 (for a-IgG molecular weight 160 kDa).

2.3 Optical setup

An optical setup based on attenuated total reflection (ATR) method with Kretschmann configuration was employed. As depicted in Fig. 1(a), He-Ne laser beam at the wavelength of $\lambda_{ex} = 633$ nm was launched to a 90° LASFN9 glass prism. On the prism base, a sensor chip for the excitation of LRSPs or regular SPs was optically matched, see Fig. 1(b). The intensity of the laser beam reflected from the prism base was measured with a photodiode detector and a lock-in amplifier (Model 5210, Princeton Applied Research, USA). Fluorescence light emitted from the surface at the wavelength of $\lambda_{em} = 670$ nm was coupled to an optical fiber by using a collimator (F220SMA-B, Thorlabs, Germany) and its intensity was detected by a photomultiplier tube (H6240-01, Hamamatsu, Japan) which was connected to a counter (53131A, Agilent, USA). The prism and detectors were mounted on a two-circle rotation

stage (Huber GmbH, Germany) in order to control the angle of incidence of the laser beam θ_I (wavelength λ_{ex}) and the angle θ_F at which the fluorescence light was collected (wavelength λ_{em}). A set of filters including edgepass filter (FES0650, Thorlabs, Germany), notch filter (XNF-632.8-25.0M, CVI Melles Griot, Germany) and band-pass filter (670FS10-25, LOT-Oriel, Germany) was used in order to suppress the background signal. The optical setup was controlled with a software Wasplas (developed at Max Plank Institute for Polymer Research in Mainz, Germany) and it allowed recording angular spectra of the reflectivity $R(\theta_I)$ and fluorescence intensity $F(\theta_I, \theta_F)$ at wavelengths λ_{ex} and λ_{em}, respectively. The fluorescence light emitted via LRSP and regular SP waves forms a characteristic cone centered at a (polar) angle θ_F for which surface plasmon modes are out-coupled by reverse Kretschmann configuration. A cross-section of the cone was measured for the azimuth angle fixed at $\phi = 0$ (see Fig. 2).
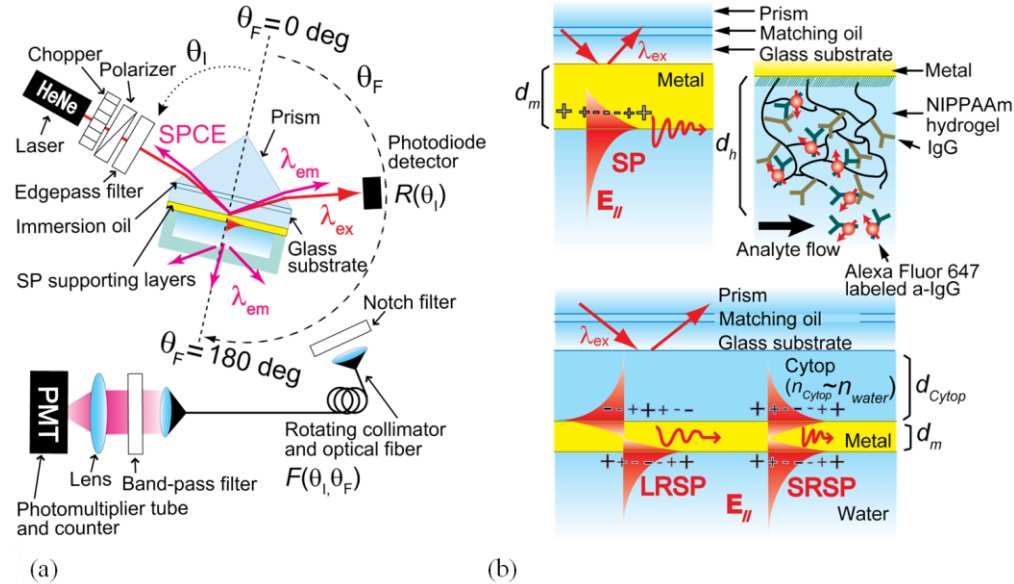
Fig. 1. (a) Optical setup for the measurement of fluorescence intensity $F(\theta_I, \theta_F)$ and reflectivity $R(\theta_I)$ angular spectra. (b) Layer architectures supporting regular SPs and LRSPs with a hydrogel binding matrix.

For the measurement of angular reflectivity spectra $R(\theta_I)$ at wavelengths λ_{ex} and λ_{em}, we used a modified setup where the laser light source and photodiode detector were replaced with a halogen lamp coupled to an optical fiber with a collimator producing a parallel polychromatic beam and with a spectrometer (HR4000 from Ocean Optics, USA), respectively. Refractive indices of gold films supporting LRSP and regular SP waves were obtained by fitting measured reflectivity curves $R(\theta_I)$ by using transfer matrix-based Fresnel reflectivity model (see Fig. 3) which was implemented in the software Winspall (developed at Max Planck Institute for Polymer Research in Mainz, Germany). The refractive indices of a gold film on Cytop polymer were $n_{Au}(\lambda_{em}) = 0.128 + 2.65i$ and $n_{Au}(\lambda_{ex}) = 0.2 + 2.68i$. The refractive indices of gold film on a glass substrate were determined as $n_{Au}(\lambda_{em}) = 0.118 + 3.92i$ and $n_{Au}(\lambda_{ex}) = 0.153 + 3.52i$ which differ from those on the Cytop surface due to a different morphology [17]. In further simulations, refractive indices of LASFN9 glass n_p, Cytop polymer n_{Cytop}, and buffer n_s at the emission and excitation wavelengths were taken from the literature as $n_p(\lambda_{em}) = 1.841$, $n_p(\lambda_{ex}) = 1.845$, $n_{Cytop}(\lambda_{em}) = 1.336$, $n_{Cytop}(\lambda_{ex}) = 1.337$, $n_s(\lambda_{em}) = 1.331$ and $n_s(\lambda_{ex}) = 1.332$ [17,20]. Refractive index of hydrogel matrix was assumed to be $n_h(\lambda_{ex}, \lambda_{em}) = 1.35$ [19].

2.4 Simulations

The classical theory of fluorescence near a metal surface [21,22] was employed for the simulation of fluorescence intensity F emitted from the hydrogel binding matrix. In these simulations, we assumed homogenously distributed, randomly oriented and identical dye molecules that were represented as oscillating emission and absorption dipoles. The orientation of emission dipole moment $\mathbf{\mu}_{em}$ was defined by polar α and azimuth β angles as shown in Fig. 2. A relative angle between the emission $\mathbf{\mu}_{em}$ and excitation $\mathbf{\mu}_{ex}$ dipole moments γ was assumed in order to take into account the structure of the dye molecule. This angle is between 0 ($\mathbf{\mu}_{em}$ and $\mathbf{\mu}_{ex}$ are parallel) and 90 deg ($\mathbf{\mu}_{em}$ and $\mathbf{\mu}_{ex}$ are perpendicular). In the model, rotation of dye molecules upon the emission was omitted. This assumption is reasonable as organic dyes were attached to a large protein which rotates much slower (characteristic time >10 ns) compared to the lifetime of excited dye ($\tau = 1$ ns for Alexa Fluor 647 according to the manufacturer). Therefore, the excitation dipole $\mathbf{\mu}_{ex}$ lying on a cone with the axis parallel to $\mathbf{\mu}_{em}$, fixed aperture 2γ and an azimuth angle ρ between 0 and 360 deg was used. The spatial position of a dipole was described by its distance from the metal surface t.
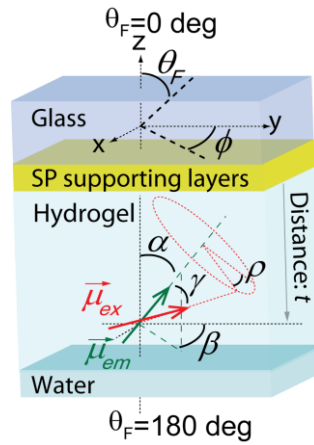
Fig. 2. Multilayer system and definition of coordinate system.

By averaging over all possible dipole orientations α, β and ρ and distances t, the fluorescence intensity F emitted at the wavelength λ_{em} to the solid angle $d\Omega = \sin(\theta_F)d\theta_F d\phi$ was obtained as:

$$F(\theta_I, \theta_F, \phi)d\Omega \propto \int P_{ex} \frac{P_{em}}{P_{tot} + P_{nr}} d\alpha \; d\beta \; d\rho \; dt \; d\Omega, \tag{1}$$

where θ_F and ϕ are fluorescence emission polar and azimuth angles, respectively, P_{ex} is the excitation rate due to the absorption of photons at the wavelength λ_{ex}, P_{em} is the emission rate that is accompanied with emitting photons at the wavelength λ_{em} and P_{nr} is the non-radiative decay rate with which the excited dye relaxes to the grounds state without emitting a photon. P_{tot} is the total radiative dissipation rate to all propagating and evanescent waves at the emission wavelength λ_{em}. The excitation rate P_{ex} was obtained as:

$$P_{ex}(t, \alpha, \beta, \theta_I) \propto \left| \mathbf{\mu}_{ex}(\alpha, \beta) \cdot \mathbf{E}_{ex}(\theta_I, t) \right|^2, \tag{2}$$

where $\mathbf{E}_{ex}$ is the electric field amplitude at distance t from the metal surface upon the excitation plane wave at the wavelength λ_{ex} hits the surface under an angle θ_I. The emission rate $P_{em}(\theta_F, \phi, t, \alpha, \beta)$ was calculated by using the transfer matrix-based model described by Polerecky et al. [23]. The non-radiative decay rate was described as $P_{nr} = P_{tot}(1/\eta - 1)$ where P_{tot}

for $t \to \infty$ was used (which corresponds to a dye immersed in water). For a dye in the proximity to a metal film, the total radiative energy dissipation rate P_{tot} is altered by additional emission channels associated with coupling to optical waves propagating along its surface. P_{tot} was obtained as a function of distance t by using the theory described by Ford et al. [22] as:

$$P_{tot}(t,\alpha) = \int_0^\infty \frac{dP_{em}}{dk_{//}}(k_{//},t,\alpha)\,dk_{//}, \tag{3}$$

$$\frac{dP_{em}}{dk_{//}}(k_{//},t,\alpha) = \frac{3}{2}\frac{1}{k_h^3}\Re e\left[\frac{k_{//}}{\sqrt{k_h^2 - k_{//}^2}}\left\{\mu_{em\perp}^2\left(k_{//}^2 r_\perp^{TM}\right) + \frac{1}{2}\mu_{em//}^2\left(k_h^2 r_{//}^{TE} + \left(k_h^2 - k_{//}^2\right)r_{//}^{TM}\right)\right\}\right], \tag{4}$$

where $dP_{em}/dk_{//}$ is the energy dissipation density and $k_{//}$ is the component of the propagation constant that is parallel to the surface (e.g., $k_{//} = 2\pi/\lambda_{em}n_p\sin\theta_F$ for waves propagating in the glass and $k_{//} > 2\pi/\lambda_{em}n_p$ for evanescent lossy surface waves). The propagation constant of light in the hydrogel film is denoted as $k_h = 2\pi/\lambda_{em}n_h$. $\mu_{em\perp} = |\mu_{em}|\cos(\alpha)$ and $\mu_{em//} = |\mu_{em}|\sin(\alpha)$ are the perpendicular and parallel components of the emission dipole moment, respectively. Coefficients $r_\perp^{TM}$ and $r_{//}^{TM}$ take into account changes in perpendicular and parallel components of electric field amplitudes of transverse magnetic polarized (TM) field upon multiple reflections at the hydrogel interfaces. Similarly, the coefficient $r_{//}^{TE}$ is the amplitude change for transverse electrical (TE). These coefficients can be described by the TM reflectivity $r_{+,-}^{TM}$ and TE reflectivity $r_{+,-}^{TE}$ at the interface between hydrogel and metal (+) and at the interface between hydrogel and water (-) as follows and are discussed in more detail in [22].

$$r_\perp^{TM} = \frac{[1 + r_-^{TM}\exp(2i\sqrt{k_h^2 - k_{//}^2}\cdot(d_h - t))][1 + r_+^{TM}\exp(2i\sqrt{k_h^2 - k_{//}^2}\cdot t)]}{1 - r_-^{TM}r_+^{TM}\exp(2i\sqrt{k_h^2 - k_{//}^2}\cdot d_h)}, \tag{5a}$$

$$r_{//}^{TM} = \frac{[1 - r_-^{TM}\exp(2i\sqrt{k_h^2 - k_{//}^2}\cdot(d_h - t))][1 - r_+^{TM}\exp(2i\sqrt{k_h^2 - k_{//}^2}\cdot t)]}{1 - r_-^{TM}r_+^{TM}\exp(2i\sqrt{k_h^2 - k_{//}^2}\cdot d_h)}, \tag{5b}$$

$$r_{//}^{TE} = \frac{[1 + r_-^{TE}\exp(2i\sqrt{k_h^2 - k_{//}^2}\cdot(d_h - t))][1 + r_+^{TE}\exp(2i\sqrt{k_h^2 - k_{//}^2}\cdot t)]}{1 - r_-^{TE}r_+^{TE}\exp(2i\sqrt{k_h^2 - k_{//}^2}\cdot d_h)}. \tag{5c}$$

3. Results and discussion

3.1 Profile of probing field

As Fig. 3(a) shows, the coupling of a light beam to LRSPs and regular SPs is manifested as a resonance dip in the angular spectrum $R(\theta_I)$. In Fig. 3(b), respective profiles of electric field intensity upon the resonant coupling to LRSPs and SPs (Kretschmann configuration with $\theta_I = 48.5$ and 56.7 deg, respectively, at the wavelength λ_{ex}) are compared to those when the light beam is normal incident at the gold surface through the sample (direct excitation $\theta_I = 180$ deg). The electric field intensity $|\mathbf{E}|^2$ was normalized with the intensity of the light beam $|\mathbf{E_0}|^2$ incident through the prism (Kretschmann configuration) or through the sample (direct excitation). These data show that fields of LRSPs and regular SPs peak at the interface between the metal and hydrogel and then exponentially decay through the hydrogel in the aqueous medium. LRSP mode exhibits a penetration depth of $L_p = 542$ nm and average field intensity enhancement of $|\mathbf{E}|^2_{ave}/|\mathbf{E_0}|^2 = 37$ in the hydrogel matrix with the thickness of $d_h = 600$ nm. Let us note that the penetration depth L_p is defined as the distance at which the amplitude of the evanescent field drops by the factor of 1/e and the average field intensity was calculated as:

$$\left|\mathbf{E}\right|^2_{ave} = \frac{1}{d_h} \int_0^{d_h} \left|\mathbf{E}(t)\right|^2 dt. \tag{6}$$

The excitation of regular SPs is associated with lower average electric field intensity enhancement of $|\mathbf{E}|^2_{ave}/|\mathbf{E_0}|^2 = 8$ as its penetration depth $L_p = 180$ nm and maximum field intensity enhancement are smaller than those for LRSP. Directly incident light beam is reflected at the gold surface and the interference gives rise to an oscillating field intensity profile with average intensity enhancement of $|\mathbf{E}|^2_{ave}/|\mathbf{E_0}|^2 = 1.3$ and $|\mathbf{E}|^2_{ave}/|\mathbf{E_0}|^2 = 2.0$ on substrates supporting LRSPs and regular SPs, respectively.
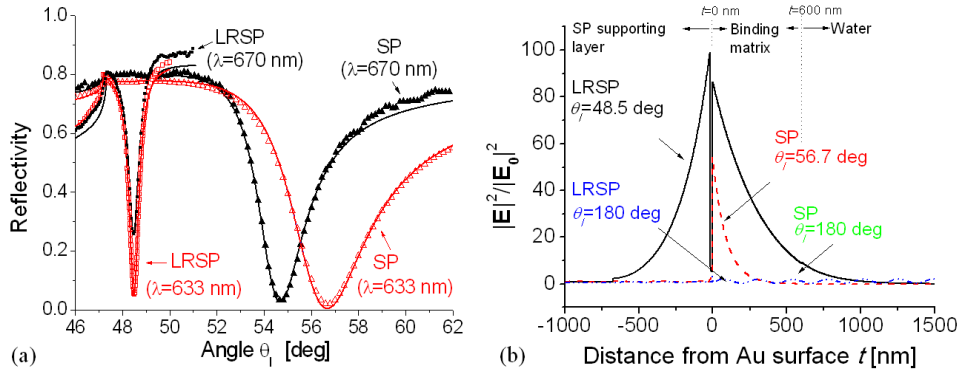
Fig. 3. (a) Angular reflectivity spectra measured for the excitation of LRSP (■, □) and SP modes (▲, △) at wavelengths of $\lambda_{em} = 670$ nm (filled) and $\lambda_{ex} = 633$ nm (blank). Lines denote the fitted curves. (b) Simulated electric field intensity profile at the wavelength $\lambda_{ex} = 633$ nm upon the resonant coupling of LRSPs ($\theta_I = 48.5$ deg, solid line) and SPs ($\theta_I = 56.7$ deg , dashed line) compared to that of directly incident light ($\theta_I = 180$, LRSP: dotted line and SP: dashed dot line).

3.2 Emission via surface plasmon waves

After the excitation, dyes in vicinity to a metal surface can emit photons via surface plasmon modes at the wavelength λ_{em}. These decay channels can be observed from the energy dissipation density $dP_{em}/dk_{//}$ that is presented in Fig. 4. It compares the emission dissipation density for dyes dispersed in a dielectric layer with the refractive index n_h and thickness of d_h = 20 and 600 nm on the top of the structure supporting (a) LRSPs and (b) regular SPs. The propagation constant region $0 \leq k_{//} \leq n_s k_0$ corresponds to the fluorescence emission via modes propagating away from a metal surface (far field emission). For propagation constants in the range $n_s k_0 \leq k_{//} \leq n_p k_0$, the fluorescence emission couples to waves that are evanescent in the sample and propagating in the glass. For larger propagation constants $k_{//} > k_0 n_p$, the fluorescence is emitted via waves that are evanescent to both glass and the sample and they contribute to the dissipation of fluorescent light in the metal (quenching).

The emission via surface plasmon modes is manifested as a series of peaks in the energy dissipation density located at distinct $k_{//}$. The emission via LRSPs (1) is manifested as a narrower peak that is located at smaller $k_{//}$ with respect to the one for regular SPs (2). In addition, one can see the emission via other modes including surface plasmons propagating at the interface between glass and gold (3) and short range surface plasmons (SRSPs) (4). For the dipole-loaded layer with the thickness of $d_h = 600$ nm, the peak energy dissipation density associated with the coupling to LRSPs is 10.6 fold higher compared to that with regular SPs. For a thinner layer with a thickness of $d_h = 20$ nm, the LRSP peak energy dissipation density is 2.2 fold higher that for the SP.
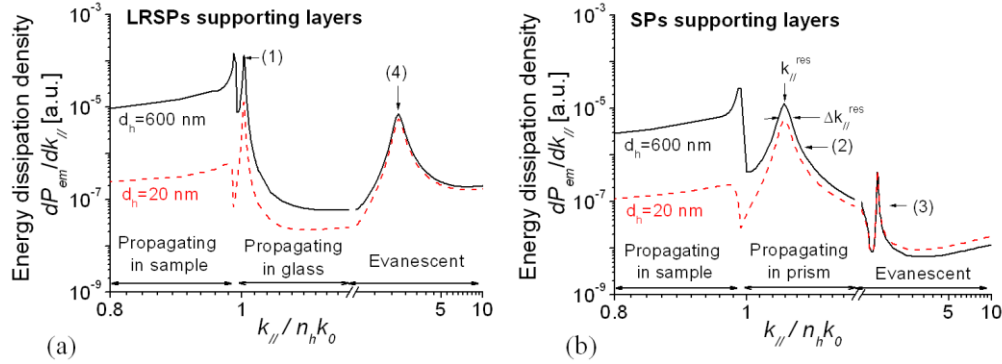
Fig. 4. Simulated energy dissipation density as a function of parallel component of the propagation constant $k_{//}$ for the binding matrix with the thickness $d_h = 20$ nm (red) and 600 nm (black) on the top of a layer structure supporting (a) LRSP and (b) regular SP modes.

Figure 5 presents the dependence of the energy dissipation probabilities $D(t)$ via regular SP, LRSP and SRSP modes on the distance t between a randomly oriented dye and the metal surface. The energy dissipation probability was calculated as:

$$D(t) = \int_0^{2\pi} \int_{-3/2\Delta k_{//}^{res}}^{3/2\Delta k_{//}^{res}} \frac{1}{P_{tot}(t,\alpha)} \frac{dP_{em}}{dk_{//}} \left(k_{//} - k_{//}^{res}, t, \alpha \right) d\alpha \, dk_{//}, \qquad (7)$$

where $k_{//}^{res}$ is the propagation constant at which the coupling to respective mode occurs and $\Delta k_{//}$ is the full width in the half maximum of the peak in the energy dissipation density [see Fig. 4(b)]. As seen in Fig. 5, the coupling efficiency to SRSPs has the maximum at distances around $t = 10$ nm (where more than 90% of fluorescence light is emitted via this mode) and it rapidly decreases for $t > 20$ nm. As SRSPs cannot be out-coupled by the used reverse Kretschmann configuration, the emission via these modes enhances quenching of the fluorescence. For regular SPs, the maximum emission probability of around 60% occurs at distances around $t = 20$ nm. The emission of fluorescence light is coupled weaker to LRSP mode and reaches its maximum of around 20% at $t = 60$ nm from the metal surface.
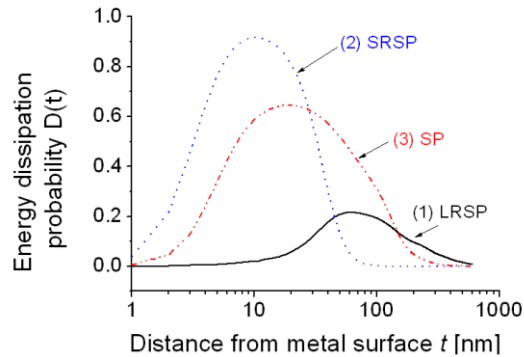
Fig. 5. The dependence of energy dissipation probability on the distance from a gold surface t. The probabilities through surface plasmon waves (LRSP: (1), SP: (3)) that can be recovered by reverse Kretschmann configuration $n_h k_0 \leq k_{//} \leq n_p k_0$ and that of SRSP which is a part of lossy wave are plotted (2).

For dyes distributed in the hydrogel, the average energy dissipation probability of via different surface plasmon modes was obtained by integrating respective $D(t)$:

$$D_{ave} = \frac{1}{d_h} \int_0^{d_h} D(t)dt. \tag{8}$$

For LRSP, the average energy dissipation probability for dyes dispersed in a 600 nm thick hydrogel matrix reaches $D_{ave} = 7\%$ which is comparable to that for regular SPs ($D_{ave} = 11\%$) and SRSPs ($D_{ave} = 5\%$), respectively. These data illustrate the balance between the effect of surface plasmon field confinement (enabling more efficient collecting of fluorescence light from a tight volume) and the thickness of the binding matrix (that can accommodate larger amount of molecules and can provide to stronger fluorescence signals).

3.3 Out-coupling of fluorescence light emitted through LRSP and SP modes

The excitation and out-coupling of fluorescence light via LRSPs and SPs modes was experimentally observed and compared with simulations. Firstly, dye-labeled biomolecules captured in a 600 nm thick binding matrix were directly excited by a laser beam normal incident at the gold surface ($\theta_I = 180$ deg) and the fluorescence intensity $F(\theta_F)$ emitted through the prism was measured. As Fig. 6(a) shows, the fluorescence light emitted via LRSP and SP modes gives rise to distinct peaks in $F(\theta_F)$ spectra centered at angles $\theta_F = 49.3$ and 56.5 deg, respectively. In the experiment, the maximum fluorescence intensity is about 1.9 ± 1.2 (standard deviation - SD) fold higher for LRSPs compared to that for SPs. In addition, full width at half maximum (FWHM) of the emission peak is 6-times narrower than that of SPs which is attributed to the lower damping of LRSPs. In Fig. 6(b), spectra from identical substrates were measured upon the fluorescence excitation by the enhanced field intensity of LRSP and regular SP modes. One can see that the peak fluorescence intensity was increased by a factor of 37 ± 10 (SD) for LRSPs with respect to that for direct excitation. Similarly, the measured peak fluorescence intensity was increased by a factor of 16 ± 8 (SD) for the SPs. The ratio of the peak fluorescence intensity for the excitation and emission via LRSP and regular SP was 4.4, see Fig. 6(b).
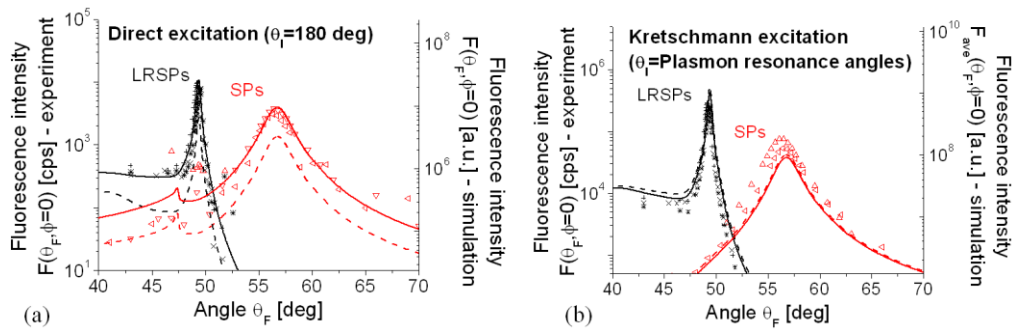
Fig. 6. Experimental fluorescence intensity emitted via LRSP and SP modes for (a) direct excitation with a laser beam ($\theta_I = 180$ deg) and (b) for the excitation via LRSP and SP modes. In each experiment, three samples were measured (black symbols for LRSPs and red symbols for SPs) and compared to the simulations with the relative angles $\gamma = 0$ and 45 deg (dashed and solid lines, respectively).

In the simulations, for the relative angle between the emission and absorption dipole $\gamma = 0$, the enhancement of peak fluorescence intensity F upon the excitation by LRSP and regular SPs is significantly larger (197-fold and 31-fold, respectively) and it decreases to 44 and 10, respectively, when increasing to the relative angle to $\gamma = 45$ deg. As the structure and the relative angle of used Alexa Fluor 647 dye are not known, this parameter was varied to match simulations with experimental data. The data presented in Fig. 6 reveal good agreement between experimental and simulation curves for γ close to 45 deg. Additional small discrepancies can be attributed to the inhomogeneous distribution of a-IgG in the hydrogel film. The used NIPAAm-base hydrogel was reported to exhibit higher density in vicinity to

the metal surface compared to the outer interface with a sample [24] and thus the density of dyes attached to individual IgG molecules is likely gradually decreasing when increasing the distance from the metal surface. Lastly, let us note that the measured enhancements for the excitation of the fluorescence light intensity via LRSPs and regular SPs, respectively, are comparable to the calculated average field intensity enhancement of $/\mathbf{E}/^2_{ave}//\mathbf{E_0}/^2 = 37$ and 8, respectively. However, the presented work shows that besides increasing the excitation rate by large field intensity enhancement, also careful design of fluorescence decay channels needs to be addressed in order to achieve maximum sensitivity of fluorescence light detection.

4. Conclusions

We investigated the long range surface plasmon-assisted excitation and emission of fluorophore-labeled molecules captured in a large-binding capacity hydrogel matrix. These surface plasmon modes offer the advantage of lower damping, more extended profile of electromagnetic field and higher field intensity enhancement with respect to regular surface plasmons. The obtained experimental data measured by using the ATR method with Kretschmann configuration exhibited good agreement with simulations. It revealed that, compared to regular surface plasmons, the combined excitation and emission via long range surface plasmons allowed increasing the peak fluorescence intensity with a factor of 4.4 and squeezing the emission in a cone that exhibited 6-fold narrower full width in half maximum. The results indicate that probing the hydrogel interface by LRSPs and regular SPs leads to similar total fluorescence light intensity collected through the surface plasmon-coupled emission. However, the employing of LRSPs offers the advantage of excitation and emission at lower angles which can simplify the implementation of this method to practical biosensor devices. In addition, the highly directional emission manifested as a narrow emission peak can be more efficiently filtered from the background signal and it can be useful for e.g. angular multiplexing of sensing channels. Our future work will be devoted to the suppressing of competing emission via LRSPs and SRSPs modes by using (nano)structured metallic films and to the implementation of combined SPFS and SPCE with LRSP modes to compact biosensor devices.